DOI 10.1002/2018JC013766

Overview of the Arctic Sea State and Boundary Layer Physics Program

Jim Thomson[1*], Stephen Ackley[2], Fanny Girard-Ardhuin[3], Fabrice Ardhuin[3], Alex Babanin[4], Guillaume Boutin[3], John Brozena[5], Sukun Cheng[6], Clarence Collins[7], Martin Doble[8], Chris Fairall[9,10], Peter Guest[11], Claus Gebhardt[12], Johannes Gemmrich[13], Hans C. Graber[14], Benjamin Holt[15], Susanne Lehner[12], Björn Lund[14], Michael H. Meylan[16], Ted Maksym[17], Fabien Montiel[18], Will Perrie[19], Ola Persson[9, 10], Luc Rainville[1], W. Erick Rogers[20], Hui Shen[19], Hayley Shen[6], Vernon Squire[18], Sharon Stammerjohn[21], Justin Stopa[3], Madison M. Smith[1], Peter Sutherland[3], Peter Wadhams[22]

[1]Applied Physics Laboratory, University of Washington, Seattle, WA, USA

[2]Snow and Ice Geophysics Laboratory, UTSA, San Antonio, TX, USA

[3]Univ. Brest, CNRS, IRD, Ifremer, Laboratoire d'Océanographie Physique et Spatiale (LOPS), IUEM, Brest, France

[4]University of Melbourne, Melbourne, VIC, Australia

[5]Marine Geosciences Division, Naval Research Laboratory, Washington, DC, USA

[6]Department of Civil and Environmental Engineering, Clarkson University, Potsdam, NY, USA

[7]Coastal and Hydraulics Laboratory, U.S. Army Engineer Research and Development Center, Duck, NC, USA

[8]Polar Scientific, Ltd, Argyll, UK

[9]CIRES/University of Colorado, Boulder, CO, USA

[10]National Oceanographic and Atmospheric Administration/Physical Sciences Division, Boulder, CO, USA

[11]Department of Meteorology, Naval Postgraduate School, Monterey, CA, USA

[12]SAR Oceanography, German Aerospace Center (DLR), Bremen, Germany

[13]Physics and Astronomy, University of Victoria, Victoria, BC, Canada

[14]University of Miami, Center for Southeastern Tropical Advanced Remote Sensing (CSTARS), Miami, Florida, USA

[15]Jet Propulsion Laboratory, California Institute of Technology, Pasadena, CA, USA

[16]School of Mathematical and Physical Sciences, University of Newcastle, Callaghan, NSW, Australia

[17]Woods Hole Oceanographic Institution, Woods Hole, MA, USA

[18]Department of Mathematics and Statistics, University of Otago, Dunedin, New Zealand

[19]Fisheries & Oceans Canada and Bedford Institute of Oceanography, Dartmouth, NS, Canada

[20]Naval Research Laboratory, Stennis Space Center, Hancock, MS, USA

[21]Institute of Arctic and Alpine Research, University of Colorado Boulder, Boulder, CO, USA

[22]Cambridge University, Cambridge, UK

[*]Correspondence to: J. Thomson, jthomson@apl.uw.edu

Received: Jan 10, 2018; Revised: Mar 21, 2018; Accepted: Mar 27, 2018

Key Points

- A large study of air-ice-ocean-waves interactions was completed during the autumn of 2015 in the western Arctic
- Strong wave-ice feedbacks, including pancake ice formation and wave attenuation, were observed
- Autumn refreezing of the seasonal ice cover is controlled by ocean preconditioning, atmospheric forcing (i.e., on-ice versus off-ice winds), and mixing events

Keywords: Arctic, waves, autumn, sea ice, Beaufort, flux

Abstract

A large collaborative program has studied the coupled air-ice-ocean-wave processes occurring in the Arctic during the autumn ice advance. The program included a field campaign in the western Arctic during the autumn of 2015, with in situ data collection and both aerial and satellite remote sensing. Many of the analyses have focused on using and improving forecast models. Summarizing and synthesizing the results from a series of separate papers, the overall view is of an Arctic shifting to a more seasonal system. The dramatic increase in open water extent and duration in the autumn means that large surface waves and significant surface heat fluxes are now common. When refreezing finally does occur, it is a highly variable process in space and time. Wind and wave events drive episodic advances and retreats of the ice edge, with associated variations in sea ice formation types (e.g., pancakes, nilas). This variability becomes imprinted on the winter ice cover, which in turn affects the melt season the following year.

1 Introduction

The western Arctic has undergone significant changes in recent decades. Perennial ice cover has been dramatically reduced, and the seasonal ice zone has expanded. This has been widely reported in the literature [e.g., *Jeffries et al.*, 2013; *Wang and Allard*, 2012; *Serreze et al.*, 2016], with many investigations on the consequences of the changing Arctic climate and inter-annual feedbacks [*Maslanik et al.*, 2007]. The Sea State and Boundary Layer Physics of the Emerging Arctic Program sponsored by the Office of Naval Research was designed to examine the specific role of surface waves and winds in the new Arctic, with a focus on the autumn refreezing period. Preliminary results from this program have been reported in *Thomson et al.* [2017] and *Lee and Thomson* [2017]. Here, we link together a series of papers in a special issue detailing many key results from the program.

1.1 Program objectives

The original objectives of the Arctic Sea State program were described in a science plan [*Thomson et al.*, 2013], as:

- Understanding the changing surface wave and wind climate in the western Arctic,
- Improving numerical and theoretical models of wave-ice interactions,
- Quantifying the fluxes of heat and momentum at the air-ice-ocean interface, and
- Applying the results in coupled forecast models.

Central to the program was a field campaign in the autumn of 2015 aboard the R/V Sikuliaq. The data collection was designed to address the objectives above, with a particular focus on data for validation and calibration of process representation in models. These models can then be used both for analysis and forecasting, as well for reanalysis (hindcast) of the changes occurring in recent decades. The data are also critical for validating new remote sensing techniques which can then provide extensive coverage of waves, ice or ocean parameters.

1.2 Climatology and context

There is a clear trend of increasing surface wave activity in the western Arctic [*Francis et al.*, 2011; *Wang et al.*, 2015; *Liu et al.*, 2016; *Thomson et al.*, 2016; *Stopa et al.*, 2016]. As shown in Figure 1, the increases are both in terms of wave height and wave period. An increase in the wind forcing, however, has not been observed. The signals are consistent with the simple explanation of increasing fetch, because more open water means more room for waves to grow [*Thomson and Rogers*, 2014; *Smith and Thomson*, 2016].

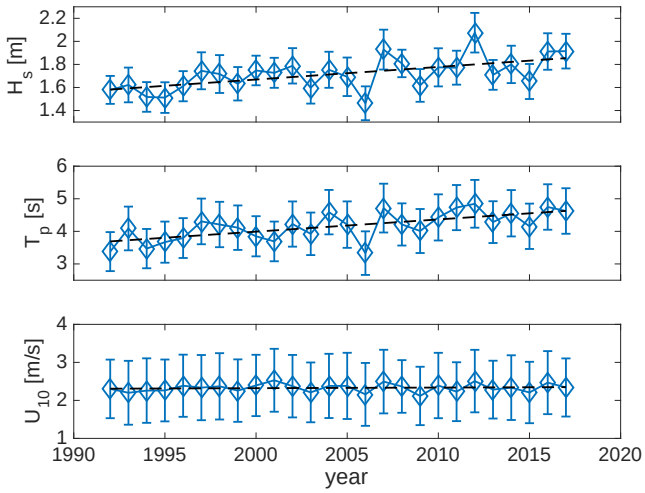

Figure 1. Trends in the wave heights, wave periods, and wind speeds over the Beaufort and Chukchi seas in autumn. Updated from [*Thomson et al.*, 2016] with values for 2015, 2016, and 2017. Values are the shape and scale parameter of Weibull distributions fit to hindcast waves across the months of September, October, and November.

Recently, some investigations have even considered the nearly unlimited fetches that would occur in an ice-free Arctic [*Li*, 2016].

Coincident with the increasing wave activity from the presence of more open water is an increase in ocean heating from solar radiation [*Perovich et al.*, 2007]. This is particularly important during years of early seasonal ice melt, as that may delay refreezing in the fall [*Stroeve et al.*, 2016]. *Stammerjohn et al.* [2012] have shown that the delay of autumn refreezing throughout the domain is both a cause and an effect of this increased ocean heating. The increased heating has led to the seasonal formation of a 'Near-Surface Temperature Maximum [NSTM, *Jackson et al.*, 2010] in the upper ocean, which accumulates heat throughout the open-water season. This ocean heat is either lost (via mixing and venting to the atmosphere) or trapped (via stratification) when refreezing occurs in the autumn. The timing of the seasonal refreezing is now delayed a full month later in the autumn, compared with previous decades [*Thomson et al.*, 2016]. As the timing of ice refreezing continues to shift, so does the probability of wave activity, given the higher chance of strong winds in autumn [*Pingree-Shippee et al.*, 2016] that coincide with open water.

2 Methods

2.1 In situ observations (R/V Sikuliaq cruise)

The field campaign was a 42-day research cruise on the R/V Sikuliaq, from late September to early November, 2015. Figure 2 shows the track of the ship, as well as the ice and wave conditions at end of the campaign. Supplemental material S1 is a movie version of this figure, showing the ship position and conditions throughout the entire cruise. This includes buoy deployments and a count of satellite images acquired.

The cruise used a dynamic approach, in which a rolling three-day plan was constantly updated based on the wind and wave forecast. The primary sampling modules were:

Figure 2. Map of cruise track and buoy deployments, overlaid on the ice and wave conditions at the end of the experiment. This is the final frame of a movie, which is included as Supplemental Material S1, showing the progression of the entire research cruise.

- Wave experiments, in which arrays of up to 17 wave sensing buoys were deployed for hours to days.
- Ice stations, in which ice floes were surveyed above and below using autonomous systems, and physical samples were collected. Ice Mass Balance (IMB) buoys were also deployed and left for the winter.
- Flux stations, in which surface fluxes of heat and momentum were measured from the bow of the ship while holding a heading into the wind.
- Ship surveys, in which an Underway Conductivity-Temperature-Depth (UCTD) was regularly deployed along a track. The ship surveys also include marine X-band radar wave-current-ice observations, visual ice observations, EM ice thickness measurements, ice camera recordings, continuous meteorological and flux observations, infrared radiometry, and radiosonde balloon launches.

Generally, the wave experiments took precedent whenever there was a favorable forecast for waves, and the other modules fit in around these events. Table 1 in *Cheng et al. [this issue]* summarizes the conditions for each wave experiment. The ice stations were selected to span a range of ice types, including multi-year floes. The flux stations were designed to capture both on-ice and off-ice winds over both open water and new ice. The underway surveys provide unique autumn measurements of air-ice-ocean structure and interactions in thin ice and the nearby open water. These include a 'race track' pattern repeated at the shelf break for several days near the end of the cruise. The UCTDs connect the shallow waters of the Chukchi Sea with the deep basin of the Beaufort Sea.

2.2 Remote sensing

Remote sensing was essential for the dynamic approach to the cruise plan. The Sikuliaq received several satellite images daily, mostly from RadarSat2 and TerraSAR-X. These were used to understand the ship's location relative to the sea ice, which often had a complex spatial distribution of multiple ice types and concentrations. In some cases, the images were annotated by analysts from the National Ice Center; these annotations included probable ice types and predictions of edge changes.

Figure 3 shows an example RadarSat2 image with the ship's position on 4 October 2017. Supplemental material S2 is a movie of the ice drift at this location, as observed with the ship's radar through a day of working near the ice edge. The ship's radar provided much higher resolution in space and time than the approximately twice daily satellite images. *Lund et al [this issue]* apply the ship's radar data to determine ice drift velocity, which can be highly variable. The ship's radar data are also suitable for determining currents and waves [*Lund et al.*, 2015, 2017].

In addition to the satellite and shipboard systems, two manned aircraft and three unmanned aerial systems (UAS) provided additional data collection and situational awareness. The aircraft from the Naval Research Laboratory (NRL) carried LIDAR and L- and P-band SAR, in addition to visual cameras. The aircraft from NASA carried the UVASAR L-band fully polarimetric SAR only (data available at https://www.asf.alaska.edu/). The UAS carried visual cameras.

In addition to real-time planning, the remote sensing data has also been used for quantitative studies. For example, wind and wave parameters can now be readily derived

Figure 3. Example RADARSAT-2 image with ship location (green symbol). The orange line is the boundary of the US Exclusive Economic Zone (200 nm from the coast). RADARSAT-2 data and products from MacDonald, Dettwiler, and Associates Ltd., All Rights Reserved.

from SAR data in the open water [*Gemmrich et al.*, 2016; *Gebhardt et al.*, 2017], and wave heights and full spectra can now be retrieved in ice-covered regions [*Ardhuin et al.*, 2015; *Gebhardt et al.*, 2016; *Ardhuin et al.*, 2017]. That method of wave spectra retrieval in ice-covered water was adapted by *[Stopa et al, this issue]* to handle a mixture of wave and ice features, and to estimate the azimuthal cut off that is needed to correct for the blurring of wave patterns near the ice edge. This produced the first map of wave heights extending over 400 km into the ice. The spatial evolution of the wave field in off-ice wind conditions is analyzed by *[Gemmrich et al, this issue]*. Other remote sensing data includes ice classification from fully polarized SAR data *[Perrie et al, this issue]*, and wave and ice floe mapping from airborne LIDAR data [*Sutherland and Gascard*, 2016].

2.3 Modeling

Much of the early effort in the Arctic Sea State program went towards including wave-ice interactions in the operational wave forecast model WAVEWATCH III. Some of the new features were first described in *Rogers and Orzech* [2013]. These have since been refined and tuned, using the data collected during the Sikuliaq cruise [*Rogers et al.*, 2016] and previous datasets [e.g. *Ardhuin et al.*, 2016]. Prior to these efforts, the only ice scheme available in WAVEWATCH III was to treat as land any regions with ice concentrations exceeding a fixed threshold [*Tolman*, 2003], usually at 75%. This early approach did not provide any wave information in the ice, and had a detrimental effect in open water with a tendency to underestimate wave heights [e.g. *Doble and Bidlot*, 2013]. The challenge in implementing more physical wave-ice interactions has been the large range in mechanisms and theoretical models proposed for these interactions (see *Squire et al.* [1995] and *Squire* [2007] for reviews), and the large range of ice types and associated processes. Both wave scattering (conservative) and wave dissipation (non-conservative) actions must be at least considered, although one or the other may dominate in a given set of conditions. Furthermore, each of these processes may be parameterized in various ways: e.g., wave scattering as 'diffusion' in *Zhao and Shen* [2016], or using a scattering matrix which is integrated implicitly [*Ardhuin and Magne*, 2007; *The WAVEWATCH III ® Development Group*, 2016].

New models have been developed as part of this program [e.g., *Montiel et al.*, 2016], and thus there is an expanding set of schemes to implement and test in WAVEWATCH III. These are noted by 'ICn' for dissipation terms and 'ISn' for scattering terms. Recent developements are documented in the WAVEWATCH III manual [*The WAVEWATCH III ® Development Group*, 2016] and in *Collins and Rogers* [2017] for IC4, including a calibration study for the Sikuliaq cruise. Additional efforts include *Boutin et al [this issue]* and *Ardhuin et al [this issue]* with effects on ice break-up on IC2 and IS2, and implementation of the "extended Fox and Squire" model (*Mosig et al.* [2015]) in WAVEWATCH III as IC5. The various schemes are summarized in Table 1. *Collins et al.* [2017a] explore the changes in the wave dispersion relation from various physical models, and *Mosig et al.* [2015] compare several viscoelastic models. *Li et al.* [2015a] explore the sensitivities of a particular viscoelastic model.

Table 1. Wave-ice interaction schemes in WAVEWATCH III.

Scheme	Mechanism
IC0	Partial blocking, scaled by ice concentration; high concentration treated as land
IS1	Simple conservative diffusive scattering term
IS2	Floe-size dependent conservative scattering, combined with ice break-up, and anelastic and/or inelastic dissipation due to ice flexure
IC1	Simple dissipation, uniform in frequency
IC2	Basal friction, laminar and/or turbulent
IC3	Ice as viscoelastic layer [*Wang and Shen*, 2010], frequency-dependent
IC4	Assorted parametric and empirical formulae, most being frequency-dependent
IC5	Ice as viscoelastic layer [extended from *Fox and Squire*, 1994], frequency-dependent

3 Results

3.1 Atmospheric forcing

Much of the autumn ice advance is driven by the atmospheric forcing. Figure 4 shows the conditions throughout the cruise, as measured by instruments on the ship. The air was cold enough for freezing conditions throughout almost the entire cruise, but it is the full surface energy budget that controls freezing, not just sensible heat flux. The most significant influence on air temperature is the wind direction; much colder temperatures are associated with off-ice winds. Under such conditions, the lower atmosphere is cooler over the ice, producing cold-air advection by the off-ice winds over the nearby open water. The very cold, dry air can cause rapid cooling and freezing at the ocean surface *[Persson et al, this issue]*. By contrast, on-ice winds can carry relative warm air from over the ocean. In either case, the gradients between these air masses can form strong low-level jets along the ice edge *[Guest et al, this issue]*.

On-ice winds can drive significant upper ocean mixing that may delay freezing or even cause a temporary reversal of the autumn ice advance. *Smith et al [this issue]* explore one such mixing event (Wave Experiment 3, 10-13 October 2015) in great detail. Figure 5 shows example images of the surface, along with the surface forcing and fluxes. The upper image is at the beginning of the event, when frazil ice is forming, and the lower image is at the end, when the frazil ice has become pancakes and upper ocean heat released due to mixing is melting the pancakes.

While Figure 4 shows a strong correlation between wind speed and wave height (as expected), the details are obscured since the ship position varied between being in the ice, at the ice edge, or in open water during different events. Wind stress is essential both for wave growth and for momentum transfer into the ocean, and the relation of wind speed to wind stress in this environment is often sensitive to the combined ice and wave conditions. For practical purposes, this is parameterized with a drag coefficient. Determination of the drag coefficient at the air-sea-ice boundary is critical to accurate atmospheric forcing [*Martin et al.*, 2016] and to wave modeling [*Tolman and Chalikov*, 1996].

3.2 Waves

Waves were observed using freely drifting buoys during seven wave experiments (see Table 1 in *Cheng et al [this issue]*). Waves were also observed along the ship track using a LIDAR range finder mounted at the bow, for which the measurements have been Doppler corrected according to *Collins et al.* [2017b], and the ship's radar. The maximum waves observed were almost 5 m significant wave height on 12 October 2017, in the middle of Wave Experiment 3 (see Figure 4). This is the upper end of the climatology determined

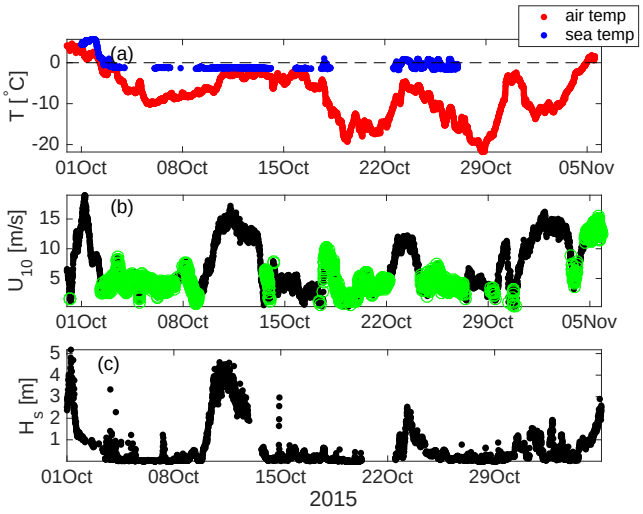

Figure 4. Time series of basic parameters along the cruise track: air and ocean temperatures (a), wind speeds (b), and wave heights (c). The green circles in (b) indicate the off-ice wind conditions. Red circles and blue circles in (a) refer to air and sea temperatures, respectively.

Figure 5. Example surface conditions and associated parameters during Wave Experiment 3 (10-12 October 2015).

Figure 6. Scaled histogram of observed in situ wave heights during the Sikuliaq cruise (black dots), compared with Weibull distributions of the hindcast wave heights throughout the domain for October of the years 2007 through 2014 (colored curves). Hindcast from *Thomson et al.* [2016].

Figure 7. Histogram of wave heights observed remotely using the TerraSAR-X satellite system during October 2015.

by *Thomson et al.* [2016] for the previous two decades. Figure 6 compares the distribution of wave heights from in situ wave observations during all wave experiments to the climatology distributions. Figure 7 shows a similar distribution of wave observations using the TerraSAR-X satellite system. The observations have peaks well above the climatology, because the adaptive sampling was targeting events with large waves. The in situ distribution (Figure 6), in particular, has a local minimum between 1 and 2 m wave heights, which is likely related to having very few samples out in open water absent a big wave event. (Wave heights of 1-2 m are now typical in the open water areas of the western Arctic.) Although these distributions reveal some sampling biases, it was not the intent to observe the climatology; the intent was to observe processes, especially those that are tied to wave-ice interactions with an increasing sea state climatology.

The full suite of wave observations have been used to determine attenuation of waves in pancake ice and then calibrate a viscoelastic model *[Cheng et al, this issue]*. This is the IC3 wave-ice scheme from Table 1, and the results suggest that elasticity is of less importance than the viscous damping. This is a consequence of pancake ice being much smaller than the wavelength; scattering is not expected to be important in this regime. *Stopa et al [this issue]* have also determined attenuation further into the ice pack during Wave Ex-

periment 3, using a larger domain thanks to wave heights derived from Sentinel 1 SAR imagery. The associated processes appear very different from what is found in pancake ice and is described by *Boutin et al [this issue]* and discussed by *Ardhuin et al [this issue]*. *Montiel and Squire [this issue]* further analyze wave attenuation and directional spreading during the large wave event of Wave Experiment 3. A key finding is that waves may tend to attenuate linearly for large amplitudes and exponentially for small amplitudes, mirroring the observations of *Kohout et al.* [2014] in the Antarctic MIZ.

Meylan et al [this issue] analyzed the power law dependence of attenuation on frequency for both measurements and models. The measurements showed universal power law dependence, being approximately four for pancake/frazil ice and two for large floes. While the models for attenuation generally have free parameters, their dependence as a function of frequency is fixed. Currently we do not know the mechanism for the energy loss. *Meylan et al [this issue]* also show how we can connect the energy loss mechanism to the power law dependence.

A consistent result from all of these approaches is that attenuation is frequency dependent, with the strongest effects at the high frequencies. This general effect has been observed in numerous prior experiments [e.g., *Collins et al.*, 2015; *Wadhams et al.*, 1988]. Data from the Sea State project provide opportunities to further quantify the low-pass filtering nature of different first-year ice types. Supplemental material S3 is a video of waves in pancake ice, in which the suppression of high frequency waves is visually apparent.

One specific issue from previous studies has been the apparent “roll-over" of attenuation at the very highest frequencies. The analyses of *Rogers et al.* [2016] did not find a roll-over for the Wave Experiment 3 and those authors speculate that cases of roll-over reported in some prior studies were spurious outcomes resulting from regeneration of wave energy by wind. Likewise, *Li et al.* [2015b] suggested that the linear rather than exponential attenuation at large wave amplitude reported for a case in Antarctic MIZ in *Kohout et al.* [2014] might also be partly due to this wind input. Most recently, *Li et al.* [2017] confirmed that roll-over in the same Antarctic case likely is a result of wind input to the highest frequencies. The wind input causes it to appear that less attenuation occurred, when comparing the net difference between two measurements (i.e., two buoys). In reality, the attenuation continues to increase with frequency. Though the above are specific case studies and results cannot be conclusively generalized to all prior wave-in-ice studies, one conclusion is unambiguous: in cases where local wind is not small, wind input *must be included* to obtain correct estimates of attenuation of wave energy by sea ice, and this is particularly crucial for estimates of the frequency-dependence of this dissipation.

Wadhams et al. [this issue] use spectra of satellite SAR images to infer attenuation and invert for pancake ice thickness. *Brozena and Sutherland [this issue]* determine attenuation rates from the airborne LIDAR and examine the importance of scattering, relative to dissipation. *Collins et al [this issue]* evaluate changes in the dispersion relation and conclude that they are small and confined to the higher wave frequencies where the wavenumber tends to increase relative to open water. This suggests, as expected, that elasticity is not important in the MIZ.

In addition to wave attenuation, wave growth is also studied with this dataset. Following *Gebhardt et al.* [2017], *Gemmrich et al. [this issue]* use TerraSAR-X wave estimates to examine fetch-limited growth of waves during off-ice wind conditions. They find mostly conventional fetch laws, with only limited evidence that waves experience any growth in partial ice cover. This is consistent with the very small wind input rates determined by *Zippel and Thomson* [2016] in partial ice cover.

Figure 8. Ice type distribution along the ship track and sample photos of each type. The size of the circles in the distribution represents the partial concentration of each type.

Figure 9. Example of multi-year ice (MYI) sampled on 6 October 2015 using UAVASAR (a,b), marine radar (c), and physical sampling (d).

Figure 10. Sea surface temperature anomaly (colors, derived from SST data available at https://mur.jpl.nasa.gov) and ice cover (grayscale, derived from AMSR2, data available at https://seaice.uni-bremen.de/start/data-archive) in the western Arctic at the start of Sikuliaq research cruise (magenta is track line).

3.3 Sea Ice

Hourly ice observations from the bridge of the ship, using the ASSIST protocols, show a wide variety of ice types and concentrations. Figure 8 shows the distribution of three dominant ice types along the cruise track. Two types are particularly common: pancake ice and nilas ice (the latter is shown as “Other " in Figure 8). These form in wavy and calm conditions, respectively. As discussed in *Thomson et al.* [2017], the observation of extensive pancake ice in the western Arctic is quite novel, and it is clearly an effect of the increasing wave climate. These ASSIST observations are complemented by a data set of shipboard images; examples are Figure 8.

Roach et al. [this issue] examine the lateral growth and welding of pancakes using in situ data, and find both processes are negatively correlated with significant wave height. The tensile stress arising from the wave field exerts a strong control on pancake size. They also evaluate lateral growth and welding predicted by parametrization schemes, which can be used to inform development of state-of-the-art sea ice models. *Lund et al [this issue]* quantify the ice drift motions, in particular the relation to the wind and the advection by ocean currents. Several studies look at the ice thickness evolution. As mentioned above, *Wadhams et al [this issue]* do this from satellite data. *Persson et al [in prep]* use a thermodynamic estimate, based on the difference between the skin temperature and the sub-surface temperature. In addition, observations of sea ice deformation features were made at six locations using an autonomous underwater vehicle, and a suite of buoys were deployed on the ice to track ice development as the fall progressed.

The program also observed multi-year floes, including the study by *Ackley et al [this issue]* which uses isotopes to understand the relative importance of snow melt and seawater, especially in melt ponds. An example of multi-year ice is shown in Figure 9.

3.4 Ocean

The western Arctic Ocean in autumn has absorbed a significant amount of heat in the preceding months. This signal however, can be very spatially heterogeneous. In 2015, a remnant tongue of ice persisted in the Beaufort Sea throughout much of the summer, and this created a region of cooler sea surface temperature in the autumn (Figure 10). This preconditioning likely influenced the progression to refreezing. Following along the ship track, significant variations in ocean heat content were observed. *Smith et al [this issue]* study the strong on-ice wind event of Wave Experiment 3 (10-13 October 2015) and show that release of stored ocean heat is sufficient to cause a temporary reversal of the autumn ice advance. Later in the cruise, the ocean heat content was particularly varied near

Figure 11. Wave height time series during Wave Experiment 3. Black dots are observations from the NIWA buoy. Colored dots are from a WAVEWATCH III hindcast using the original ice parameterization (green) and newly implemented ice parameterizations (red, blue).

Figure 12. Mean Arctic ice cover in the late 20th century (left columns) and predicted for the late 21st century (right columns) for the months of August, September, and October.

the shelf-break, where the advancing ice edge appeared to loiter, analogous to loitering of the retreating ice edge in the spring [*Steele and Ermold*, 2015]. This loitering was only disturbed by very strong cooling coincident with off-ice winds *Persson et al [this issue]*.

4 Discussion

4.1 Forecast challenges

Forecasting was crucial to the research cruise, because the timing and location of the wave experiments were planned in near real-time. The forecasts available on the ship were a combination of operational products and custom products developed as part of the larger research program. At the time of the Sikuliaq cruise, most models used only one-way coupling (or no coupling). For wave forecasting, this meant that the sea ice model was simply an input to the wave model, and the waves could not feedback to the ice. In many cases, the sensitivity to the quality (or lack) of the ice input was severe.

In a hindcast analysis, such as the wave height time series in Figure 11, the wave model can be tuned and the ice input selected to achieve good agreement with in situ wave observations. A priori, however, it can be very difficult to know which ice parameterization to choose and which ice input to use. This is further complicated by the discrepancies between ice models and ice observations (see Figures S6, S7 of *Cheng et al.* [2017]). Clearly, the new parameterizations (ICn) are superior to the original one (IC0), but there are still significant differences among the parameterizations (see Figure 11). In particular, the different parameterizations can have very different performance in replicating the spectral filtering that is often observed in ice, in which high-frequency components are attenuated and low-frequency components propagate unaltered. Further complicating the matter is that model results from WAVEWATCH III are sensitive to all source terms, not just ice, and these other source terms, in particular wind input and nonlinear interactions, may also change in the presence of ice. These source terms have been tuned in open water conditions only. Inter-dependence of these source terms has been indicated in *Cheng et al.* [2017]. This effect is obscured when examining wave heights alone, but can be crucial to questions of mixing *[Smith et al, this issue]*.

4.2 Feedbacks and future climate scenarios

The challenge in creating models capable of forecast and climate predictions is in the highly coupled nature of the air-sea-ice-wave processes [e.g., *Khon et al.*, 2014]. Although this program has produced many improvements in fundamental understanding of the coupled processes and the model representation thereof, there is still a strong need to develop better model coupling. The need is urgent, given the scenarios for extreme change in the Arctic. Figure 12 compares historical ice cover with the CIOM A1B scenario predictions for the end of this century [*Long and Perrie*, 2013, 2015, 2017]. The ice-free August is remarkable, but the October ice cover is more so because it implicates all of the processes explored in this program.

For example, pancake formation, or almost any ice type, is not included in ice models. This would almost surely involve coupling to a wave model. There is recent progress in representing the wave-forced breakup of ice into specific Floe Size Distributions [FSD, *Montiel and Squire*, 2017], that has yet to be included in any wave-ice model. A complementary avenue for progress in this area is in laboratory experiments, where interacting processes may be isolated. For example, details of the wave interactions with individual ice floes is more readily apparent [*Bennetts et al.*, 2015].

Similarly, the details of wave and wind coupling in the presence of ice are not fully understood. Although wind input is reduced in ice [*Zippel and Thomson*, 2016], there may still be sufficient wind input to offset some of the attenuation [*Li et al.*, 2015b, 2017].

The recent trend of decreasing ice cover in the fall in the Chukchi/Beaufort region exposes the relatively warm ocean surface to the atmosphere, causing deeper and more unstable atmospheric boundary layers, which results in higher winds, wind stress and turbulent heat fluxes at the surface. Also the presence of ice edges and marginal ice zones (which only existed to the south in previous decades) creates horizontal temperature gradients that can create low level wind jets, several of which were experienced during the cruise *[Guest et al., this issue; Persson et al, this issue]* . More open water will likely result in generation of previously-rare mesoscale cyclones, including Polar Lows [*Inoue et al.*, 2010], and also may result in changes to synoptic-scale cyclone storm tracks, bringing more storms into the region [*Wang et al.*, 2017]. These phenomena indicate the importance of considering atmospheric feedbacks in understanding air-ice-ocean interaction and wave generation in the Arctic.

5 Conclusions

The Arctic Sea State program has quantified the trend of increasing waves in the western Arctic and the implications for air-ice-ocean processes. In 2013 when the science plan of the Sea State program was written, it was only a conjecture that waves were becoming a significant player of the emerging Arctic in autumn freezing. Climatology suggested a big signal, but the detailed processes were not known. In 2015, the field campaign documented the extent of sea state influences on the Arctic in autumn. The most notable signal is the new prevalence of pancake ice near the ice edge, which is a direct consequence of increasing wave activity. In this sense, the Arctic may be transitioning to a state more similar to the Antarctic, where waves and pancake ice are ubiquitous.

Autumn refreezing in the western Arctic can now be summarized as a complex process controlled by:

- ocean preconditioning by air-sea heat fluxes,
- wave-ice feedbacks (e.g., pancake formation, attenuation),
- ocean cooling during off-ice winds,
- ocean mixing during on-ice winds, and
- ice edge reversals during events.

These results and the products of this program are being used to improve forecast and climate models. In addition to the challenge of two-way coupling in these models, the event-driven nature of the key processes may be difficult for model tuning (though the ample parameters measured or derived should allow model improvements through process validation techniques). This new dataset is a leap forward in autumn Arctic observations, in which one particularly large wave event was extensively measured. Of course, if events drive the system, observations of numerous events will be required to make meaningful progress in model development. Still, we expect this data set to be used extensively for future studies, such as examining details of air-ice-ocean momentum transports and air-

ice-ocean interactions during off-ice wind events, which were more common than on-ice events.

The papers contained within this special issue are the first round of analyses from the field data and model developments. As always, there is more work to be done. The data archive is available for continued analysis and model testing by an expanding set of researchers. Although key processes have been identified and quantified, much remains to be understood about the temporal and spatial scales over which these processes occur.

The complexity and variability of the upper ocean structure stands out within the dataset as a remaining challenge. Significant efforts have been ongoing for decades to understand the inflow of Pacific Summer Water (PSW) over the Chukchi slope, the circulation of the Beaufort Gyre, and the eddies that are generated near the boundaries. Even with this context and climatology, however, it was not possible to make skillful predictions of underway CTD observations during the Arctic Sea State campaign. The strength of both the near surface temperature maximum (NSTM) and the PSW were highly variable along the ship track. It is clear that the progression of the seasonal ice cover has a strong influence on this upper ocean variability, but the atmospheric and advective signals driving the sea ice itself also show considerable variability. Therefore, to understand the drivers of this tightly coupled air-sea-ice system, not only do the simultaneous air-sea-ice interactions need to be considered, but also the far field and preconditioning factors need to be addressed as well. A new program, the Stratified Ocean Dynamics in the Arctic (www.apl.uw.edu/soda) aims to understand this variability with an observational campaign over the 2018-2019 annual cycle.

The complexity of the sea ice remains another challenge. As demonstrated by the extensive visual observations following the ASPECT protocols, sea ice is not easily characterized by a few scalar parameters (though that is what coupled models would most easily use). This challenge is extreme during refreezing, when changing surface fluxes cause rapid evolution of the new sea ice (e.g., Persson et al, this issue). Models such as CICE and in situ observations must converge on a set of metrics that are most relevant to the coupled dynamics and that capture the variability. Another new program, the Sea Ice Dynamics Experiment (SIDEX) will make progress on this topic with a 2020 campaign.

Finally, though the new wave-ice schemes in models like WAVEWATCH3 are impressive in their ability to reproduce observations in a hindcast, there is still a fundamental question as the mechanism(s) by which waves lose energy as they propagate through sea ice. The new dataset is by far the most extensive observation of waves in sea ice collected to date, yet the measurements are mostly the net effect of the wave-ice interactions, and limited to the region less than 100 km from the open ocean. Direct measurements of collisions, flexure, and turbulence within pancake ice are the next horizon for measurements of wave-ice processes. To follow the evolution of these processes from the ice edge to the interior pack ice requires larger spatial monitoring. More ambitious still, the message from the Arctic Sea State program is clear: these specific interactions exist within a fully coupled air-ocean-ice system, and such measurements would be incomplete without characterizing the whole system simultaneously.

Acknowledgments

This program was supported by the Office of Naval Research, Code 32, under Program Managers Drs. Scott Harper and Martin Jeffries. The crew of R/V Sikuliaq provide outstanding support in collecting the field data, and the US National Ice Center, German Aerospace Center (DLR), and European Space Agency facilitated the remote sensing collections and daily analysis products. RADARSAT-2 Data and Products are from MacDonald, Dettwiler, and Associates Ltd., courtesy of the U.S. National Ice Center

Data, supplemental material, and a cruise report can be found at http://www.apl.uw.edu/arcticseastate

References

Ardhuin, F., and R. Magne (2007), Current effects on scattering of surface gravity waves by bottom topography, *J. Fluid Mech.*, *576*, 235–264.

Ardhuin, F., F. Collard, B. Chapron, F. Girard-Ardhuin, G. Guitton, A. Mouche, and J. E. Stopa (2015), Estimates of ocean wave heights and attenuation in sea ice using the sar wave mode on sentinel-1a, *Geophysical Research Letters*, *42*(7), 2317–2325, doi: 10.1002/2014GL062940, 2014GL062940.

Ardhuin, F., P. Sutherland, M. Doble, and P. Wadhams (2016), Ocean waves across the arctic: Attenuation due to dissipation dominates over scattering for periods longer than 19 s, *Geophysical Research Letters*, pp. n/a–n/a, doi:10.1002/2016GL068204, 2016GL068204.

Ardhuin, F., J. Stopa, B. Chapron, F. Collard, M. Smith, J. Thomson, M. Doble, B. Blomquist, O. Persson, C. O. C. III, and P. Wadhams (2017), Measuring ocean waves in sea ice using SAR imagery: A quasi-deterministic approach evaluated with Sentinel-1 and in situ data, *Remote Sensing of Environment*, *189*, 211 – 222, doi: http://dx.doi.org/10.1016/j.rse.2016.11.024.

Bennetts, L., A. Alberello, M. Meylan, C. Cavaliere, A. Babanin, and A. Toffoli (2015), An idealised experimental model of ocean surface wave transmission by an ice floe, *Ocean Modelling*, *96*(Part 1), 85 – 92, doi:https://doi.org/10.1016/j.ocemod.2015.03.001, waves and coastal, regional and global processes.

Cheng, S., W. E. Rogers, J. Thomson, M. Smith, M. J. Doble, P. Wadhams, A. L. Kohout, B. Lund, O. P. Persson, C. O. Collins, S. F. Ackley, F. Montiel, and H. H. Shen (2017), Calibrating a viscoelastic sea ice model for wave propagation in the arctic fall marginal ice zone, *Journal of Geophysical Research: Oceans*, *122*, n/a–n/a, doi: 10.1002/2017JC013275.

Collins, C., and W. Rogers (2017), A source term for wave attenuation by sea ice in WAVEWATCH III: IC4, *Tech. Rep. NRL/MR/7320–17-9726*, Naval Research Laboratory.

Collins, C. O., W. E. Rogers, A. Marchenko, and A. V. Babanin (2015), In situ measurements of an energetic wave event in the arctic marginal ice zone, *Geophysical Research Letters*, pp. n/a–n/a, doi:10.1002/2015GL063063.

Collins, C. O., W. E. Rogers, and B. Lund (2017a), An investigation into the dispersion of ocean surface waves in sea ice, *Ocean Dynamics*, *67*(2), 263–280, doi:10.1007/s10236-016-1021-4.

Collins, C. O., B. Blomquist, O. Persson, B. Lund, W. E. Rogers, J. Thomson, D. Wang, M. Smith, M. Doble, P. Wadhams, A. Kohout, C. Fairall, and H. C. Graber (2017b), Doppler correction of wave frequency spectra measured by underway vessels, *Journal of Atmospheric and Oceanic Technology*, *34*(2), 429–436, doi:10.1175/JTECH-D-16-0138.1.

Doble, M. J., and J.-R. Bidlot (2013), Wave buoy measurements at the antarctic sea ice edge compared with an enhanced ecmwf wam: Progress towards global waves-in-ice modelling, *Ocean Modelling*, *70*(Supplement C), 166 – 173, doi: https://doi.org/10.1016/j.ocemod.2013.05.012, ocean Surface Waves.

Fox, C., and V. A. Squire (1994), On the Oblique Reflexion and Transmission of Ocean Waves at Shore Fast Sea Ice, *Philosophical Transactions of the Royal Society of London Series A*, *347*, 185–218, doi:10.1098/rsta.1994.0044.

Francis, O. P., G. G. Panteleev, and D. E. Atkinson (2011), Ocean wave conditions in the Chukchi Sea from satellite and in situ observations, *Geophys. Res. Lett.*, *38*(L24610), doi:10.1029/2011GL049839.

Gebhardt, C., J.-R. Bidlot, J. Gemmrich, S. Lehner, A. Pleskachevsky, and W. Rosenthal (2016), Wave observation in the marginal ice zone with the terrasar-x satellite, *Ocean Dynamics*, *66*(6), 839–852, doi:10.1007/s10236-016-0957-8.

Gebhardt, C., J. R. Bidlot, S. Jacobsen, S. Lehner, P. O. G. Persson, and A. L. Pleskachevsky (2017), The potential of terrasar-x to observe wind wave interaction at the ice edge, *IEEE Journal of Selected Topics in Applied Earth Observations and Remote*

Sensing, *10*(6), 2799–2809, doi:10.1109/JSTARS.2017.2652124.

Gemmrich, J., J. Thomson, W. E. Rogers, A. Pleskachevsky, and S. Lehner (2016), Spatial characteristics of ocean surface waves, *Ocean Dynamics*, *66*(8), 1025–1035, doi:10.1007/s10236-016-0967-6.

Inoue, J., M. E. Hori, Y. Tachibana, and T. Kikuchi (2010), A polar low embedded in a blocking high over the pacific arctic, *Geophysical Research Letters*, *37*(14), n/a–n/a, doi:10.1029/2010GL043946, l14808.

Jackson, J. M., E. C. Carmack, F. A. McLaughlin, S. E. Allen, and R. G. Ingram (2010), Identification, characterization, and change of the near-surface temperature maximum in the canada basin, 1993–2008, *Journal of Geophysical Research: Oceans*, *115*(C5), n/a–n/a, doi:10.1029/2009JC005265, c05021.

Jeffries, M. O., J. E. Overland, and D. K. Perovich (2013), The Arctic shifts to a new normal, *Physics Today*, *66*(10), doi:10.1063/PT.3.2147.

Khon, V. C., I. I. Mokhov, F. A. Pogarskiy, A. Babanin, K. Dethloff, A. Rinke, and H. Matthes (2014), Wave heights in the 21st century arctic ocean simulated with a regional climate model, *Geophysical Research Letters*, *41*(8), 2956–2961, doi:10.1002/2014GL059847, 2014GL059847.

Kohout, A. L., M. J. M. Williams, S. M. Dean, and M. H. Meylan (2014), Storm-induced sea-ice breakup and the implications for ice extent, *Nature*, *509*, 604 EP –.

Lee, C., and J. Thomson (2017), An autonomous approach to observing the seasonal ice zone, *Oceanography Magazine*, *30*.

Li, J., S. Mondal, and H. H. Shen (2015a), Sensitivity analysis of a viscoelastic parameterization for gravity wave dispersion in ice covered seas, *Cold Regions Science and Technology*, *120*, 63 – 75, doi:https://doi.org/10.1016/j.coldregions.2015.09.009.

Li, J., A. L. Kohout, and H. H. Shen (2015b), Comparison of wave propagation through ice covers in calm and storm conditions, *Geophysical Research Letters*, *42*(14), 5935–5941, doi:10.1002/2015GL064715, 2015GL064715.

Li, J., A. L. Kohout, M. J. Doble, P. Wadhams, C. Guan, and H. H. Shen (2017), Rollover of apparent wave attenuation in ice covered seas, *Journal of Geophysical Research: Oceans*, pp. n/a–n/a, doi:10.1002/2017JC012978.

Li, J.-G. (2016), Ocean surface waves in an ice-free arctic ocean, *Ocean Dynamics*, *66*(8), 989–1004, doi:10.1007/s10236-016-0964-9.

Liu, Q., A. V. Babanin, S. Zieger, I. R. Young, and C. Guan (2016), Wind and wave climate in the arctic ocean as observed by altimeters, *Journal of Climate*, *29*(22), 7957–7975, doi:10.1175/JCLI-D-16-0219.1.

Long, Z., and W. Perrie (2013), Impacts of climate change on fresh water content and sea surface height in the Beaufort Sea, *Ocean Modelling*, *71*, 127–139, doi:http://dx.doi.org/10.1016/j.ocemod.2013.05.006.

Long, Z., and W. Perrie (2015), Scenario changes of Atlantic water in the Arctic Ocean, *J. Climate*, *28*, 552305,548, doi:http://dx.doi.org/10.1175/JCLI-D-14-00522.1.

Long, Z., and W. Perrie (2017), Changes in ocean temperature in the Barents sea in the twenty-first century, *Journal of Climate*, *30*(15), 5901–5921, doi:10.1175/JCLI-D-16-0415.1.

Lund, B., H. C. Graber, K. Hessner, and N. J. Williams (2015), On shipboard marine x-band radar near-surface current "calibration", *Journal of Atmospheric and Oceanic Technology*, *32*(10), 1928–1944, doi:10.1175/JTECH-D-14-00175.1.

Lund, B., C. J. Zappa, H. C. Graber, and A. Cifuentes-Lorenzen (2017), Shipboard wave measurements in the southern ocean, *Journal of Atmospheric and Oceanic Technology*, *34*(9), 2113–2126, doi:10.1175/JTECH-D-16-0212.1.

Martin, T., M. Tsamados, D. Schroeder, and D. L. Feltham (2016), The impact of variable sea ice roughness on changes in arctic ocean surface stress: A model study, *Journal of Geophysical Research: Oceans*, pp. n/a–n/a, doi:10.1002/2015JC011186.

Maslanik, J. A., C. Fowler, J. C. Stroeve, S. Drobot, J. Zwally, D. Yi, and W. Emery (2007), A younger, thinner Arctic ice cover: Increased potential for rapid, extensive sea-

ice loss, *Geophys. Res. Lett.*, *34*(34).

Montiel, F., and V. A. Squire (2017), Modelling wave-induced sea ice break-up in the marginal ice zone, *Proceedings of the Royal Society of London A: Mathematical, Physical and Engineering Sciences*, *473*(2206), doi:10.1098/rspa.2017.0258.

Montiel, F., V. A. Squire, and L. G. Bennetts (2016), Attentuation and directional spreading of ocean wave spectra in the marginal ice zone, *J. Fluid Mech.*, *790*, 492–522.

Mosig, J. E. M., F. Montiel, and V. A. Squire (2015), Comparison of viscoelastic-type models for ocean wave attenuation in ice-covered seas, *Journal of Geophysical Research: Oceans*, *120*(9), 6072–6090, doi:10.1002/2015JC010881.

Perovich, D. K., B. Light, H. Eicken, K. F. Jones, K. Runciman, and S. V. Nghiem (2007), Increasing solar heating of the arctic ocean and adjacent seas, 1979–2005: Attribution and role in the ice-albedo feedback, *Geophysical Research Letters*, *34*(19), n/a–n/a, doi:10.1029/2007GL031480, l19505.

Pingree-Shippee, K. A., N. J. Shippee, and D. E. Atkinson (2016), Overview of Bering and Chukchi sea wave states for four severe storms following common synoptic tracks, *Journal of Atmospheric and Oceanic Technology*, *33*(2), 283–302, doi:10.1175/JTECH-D-15-0153.1.

Rogers, W., and M. D. Orzech (2013), Implementation and testing of ice and mud source functions in WAVEWATCH III, *Memorandum Report NRL/MR/7320–13-9462*, Naval Research Laboratory.

Rogers, W. E., J. Thomson, H. H. Shen, M. J. Doble, P. Wadhams, and S. Cheng (2016), Dissipation of wind waves by pancake and frazil ice in the autumn beaufort sea, *Journal of Geophysical Research: Oceans*, *121*(11), 7991–8007, doi:10.1002/2016JC012251.

Serreze, M. C., A. D. Crawford, J. C. Stroeve, A. P. Barrett, and R. A. Woodgate (2016), Variability, trends, and predictability of seasonal sea ice retreat and advance in the chukchi sea, *Journal of Geophysical Research: Oceans*, pp. n/a–n/a, doi:10.1002/2016JC011977.

Smith, M., and J. Thomson (2016), Scaling observations of surface waves in the beaufort sea, *Elem Sci Anth*, *4*(000097), doi:10.12952/journal.elementa.000097.

Squire, V. A. (2007), Of ocean waves and sea ice revisited, *Cold Regions Sci. Tech.*, *49*, 110–133.

Squire, V. A., J. P. Dugan, P. Wadhams, P. J. Rottier, and A. K. Liu (1995), Of ocean waves and sea ice, *Annu. Rev. Fluid Mech.*, *27*, 115–168.

Stammerjohn, S., R. Massom, D. Rind, and D. Martinson (2012), Regions of rapid sea ice change: An inter-hemispheric seasonal comparison, *Geophysical Research Letters*, *39*(6), n/a–n/a, doi:10.1029/2012GL050874, l06501.

Steele, M., and W. Ermold (2015), Loitering of the retreating sea ice edge in the arctic seas, *Journal of Geophysical Research: Oceans*, *120*(12), 7699–7721, doi:10.1002/2015JC011182.

Stopa, J. E., F. Ardhuin, and F. Girard-Adrhuin (2016), Wave-climate in the Arctic 1992-2014: seasonality, trends, and wave-ice influence, *The Cryosphere*, *10*(4), 1605–1629, doi:10.5194/tc-10-1605-2016.

Stroeve, J. C., A. D. Crawford, and S. Stammerjohn (2016), Using timing of ice retreat to predict timing of fall freeze-up in the arctic, *Geophysical Research Letters*, *43*(12), 6332–6340, doi:10.1002/2016GL069314, 2016GL069314.

Sutherland, P., and J.-C. Gascard (2016), Airborne remote sensing of ocean wave directional wavenumber spectra in the marginal ice zone, *Geophysical Research Letters*, pp. n/a–n/a, doi:10.1002/2016GL067713, 2016GL067713.

The WAVEWATCH III ® Development Group (2016), User manual and system documentation of WAVEWATCH III version 5.16, *Tech. Rep. 329*, NOAA/NWS/NCEP/Marine Modeling and Analysis Branch.

Thomson, J., and W. E. Rogers (2014), Swell and sea in the emerging Arctic Ocean, *Geophysical Research Letters*, pp. n/a–n/a, doi:10.1002/2014GL059983.

Thomson, J., V. Squire, S. Ackley, E. Rogers, A. Babanin, P. Guest, T. Maksym, P. Wadhams, S. Stammerjohn, C. Fairall, O. Persson, M. Doble, H. Graber, H. Shen, J. Gemmrich, S. Lehner, B. Holt, T. Williams, M. Meylan, and J. Bidlot (2013), Science plan: Sea state and boundary layer physics of the emerging Arctic Ocean, *Technical Report 1306*, Applied Physics Laboratory, University of Washington.

Thomson, J., Y. Fan, S. Stammerjohn, J. Stopa, W. E. Rogers, F. Girard-Ardhuin, F. Ardhuin, H. Shen, W. Perrie, H. Shen, S. Ackley, A. Babanin, Q. Liu, P. Guest, T. Maksym, P. Wadhams, C. Fairall, O. Persson, M. Doble, H. Graber, B. Lund, V. Squire, J. Gemmrich, S. Lehner, B. Holt, M. Meylan, J. Brozena, and J.-R. Bidlot (2016), Emerging trends in the sea state of the beaufort and chukchi seas, *Ocean Modelling*, *105*, 1 – 12, doi:http://dx.doi.org/10.1016/j.ocemod.2016.02.009.

Thomson, J., S. Ackley, H. H. Shen, and W. E. Rogers (2017), The balance of ice, waves, and winds in the arctic autumn, *Eos*, *98*, doi:https://doi.org/10.1029/2017EO066029.

Tolman, H. L. (2003), Treatment of unresolved islands and ice in wind wave models, *Ocean Modeling*, *5*, 219–231.

Tolman, H. L., and D. Chalikov (1996), Source terms in a third-generation wind wave model, *Journal of Physical Oceanography*, *26*(11), 2497–2518, doi:10.1175/1520-0485(1996)026<2497:STIATG>2.0.CO;2.

Wadhams, P., V. A. Squire, D. J. Goodman, A. M. Cowan, and S. C. Moore (1988), The attenuation rates of ocean waves in the marginal ice zone, *J. Geophys. Res*, *93*(C6), 6799–6818.

Wang, D., and R. Allard (2012), Validation of the operational performance of NAVO SHARC METOC and wave sensor systems, *Tech. rep.*, Naval Research Laboratory.

Wang, J., H.-M. Kim, and E. K. M. Chang (2017), Changes in northern hemisphere winter storm tracks under the background of arctic amplification, *Journal of Climate*, *30*(10), 3705–3724, doi:10.1175/JCLI-D-16-0650.1.

Wang, R., and H. H. Shen (2010), Gravity waves propagating into an ice-covered ocean: A viscoelastic model, *Journal of Geophysical Research: Oceans*, *115*(C6), n/a–n/a, doi:10.1029/2009JC005591, c06024.

Wang, X. L., Y. Feng, V. R. Swail, and A. Cox (2015), Historical changes in the Beaufort-Chukchi-Bering seas surface winds and waves, 1971-2013, *Journal of Climate*, doi:10.1175/JCLI-D-15-0190.1.

Zhao, X., and H. Shen (2016), A diffusion approximation for ocean wave scatterings by randomly distributed ice floes, *Ocean Modelling*, *107*, 21 – 27, doi:https://doi.org/10.1016/j.ocemod.2016.09.014.

Zippel, S., and J. Thomson (2016), Air-sea interactions in the marginal ice zone, *Elem Sci Anth*, *4*(000095).

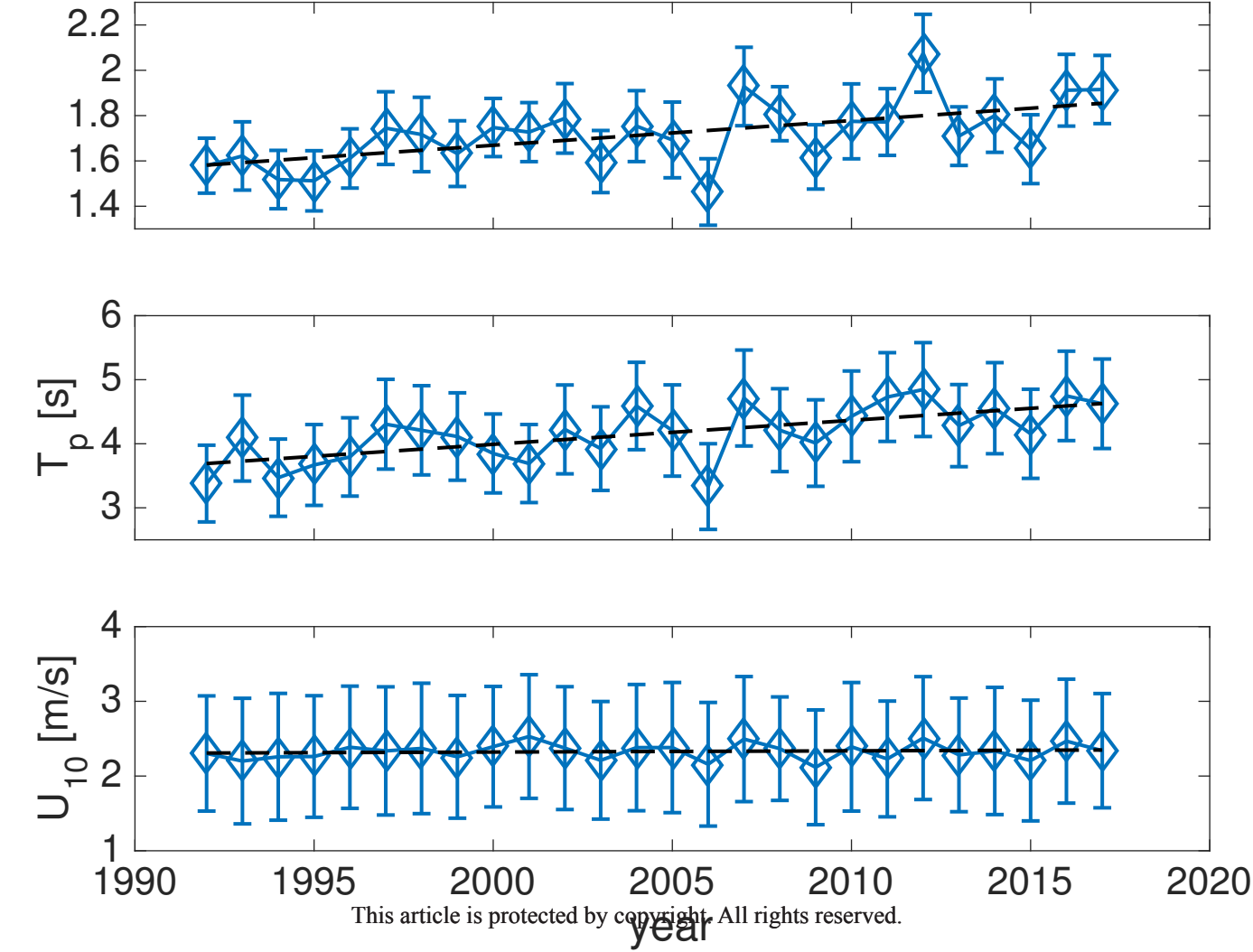

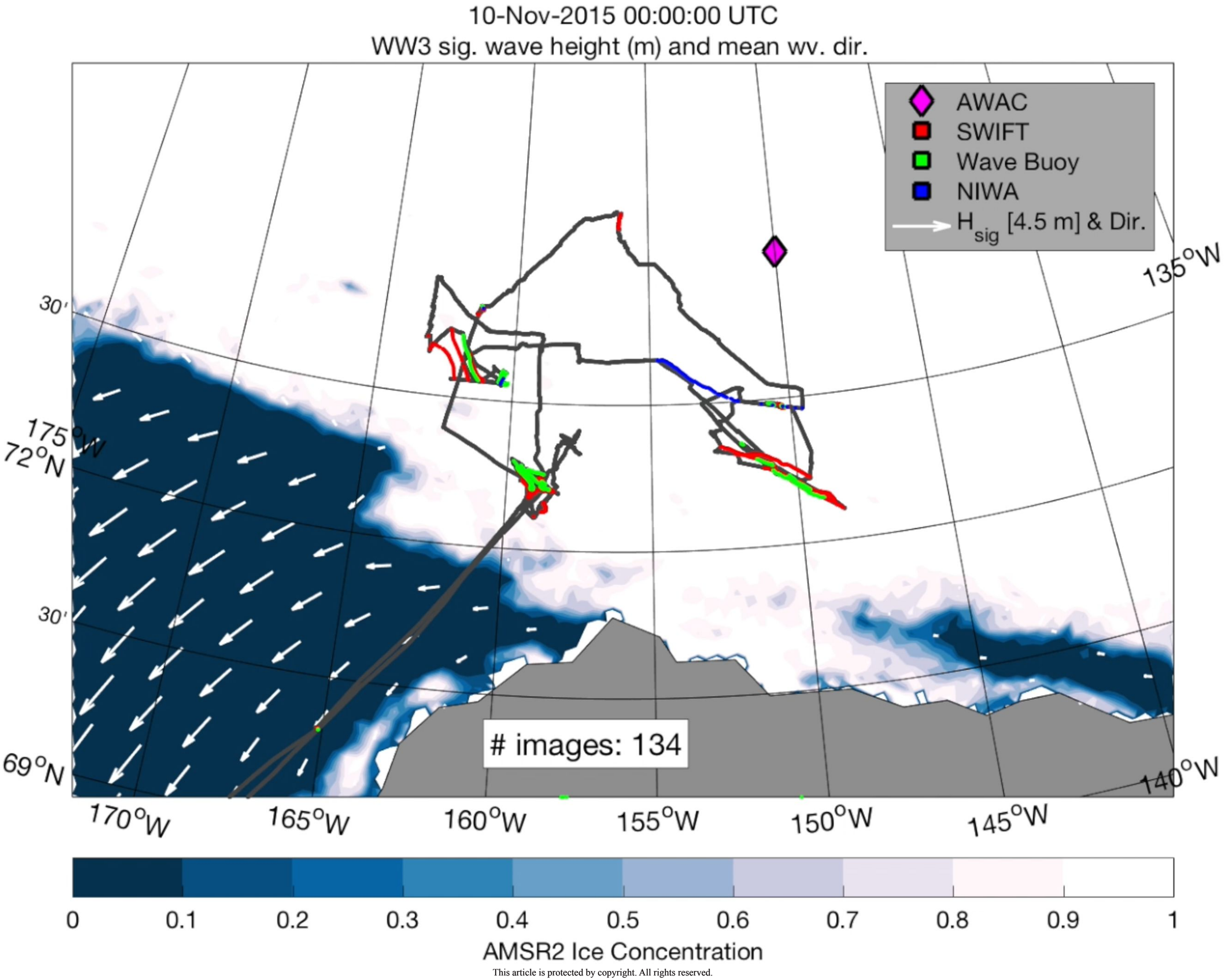

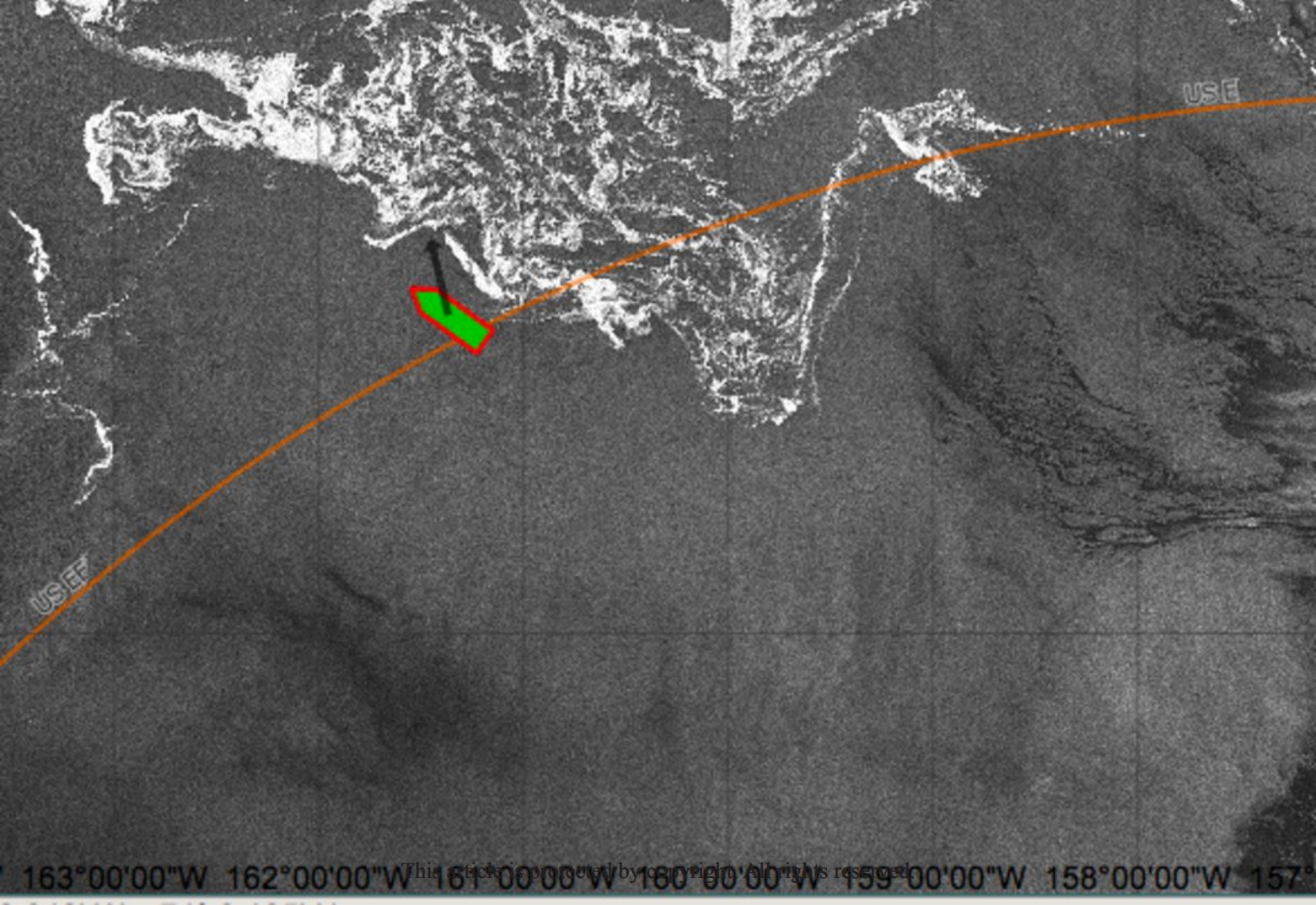

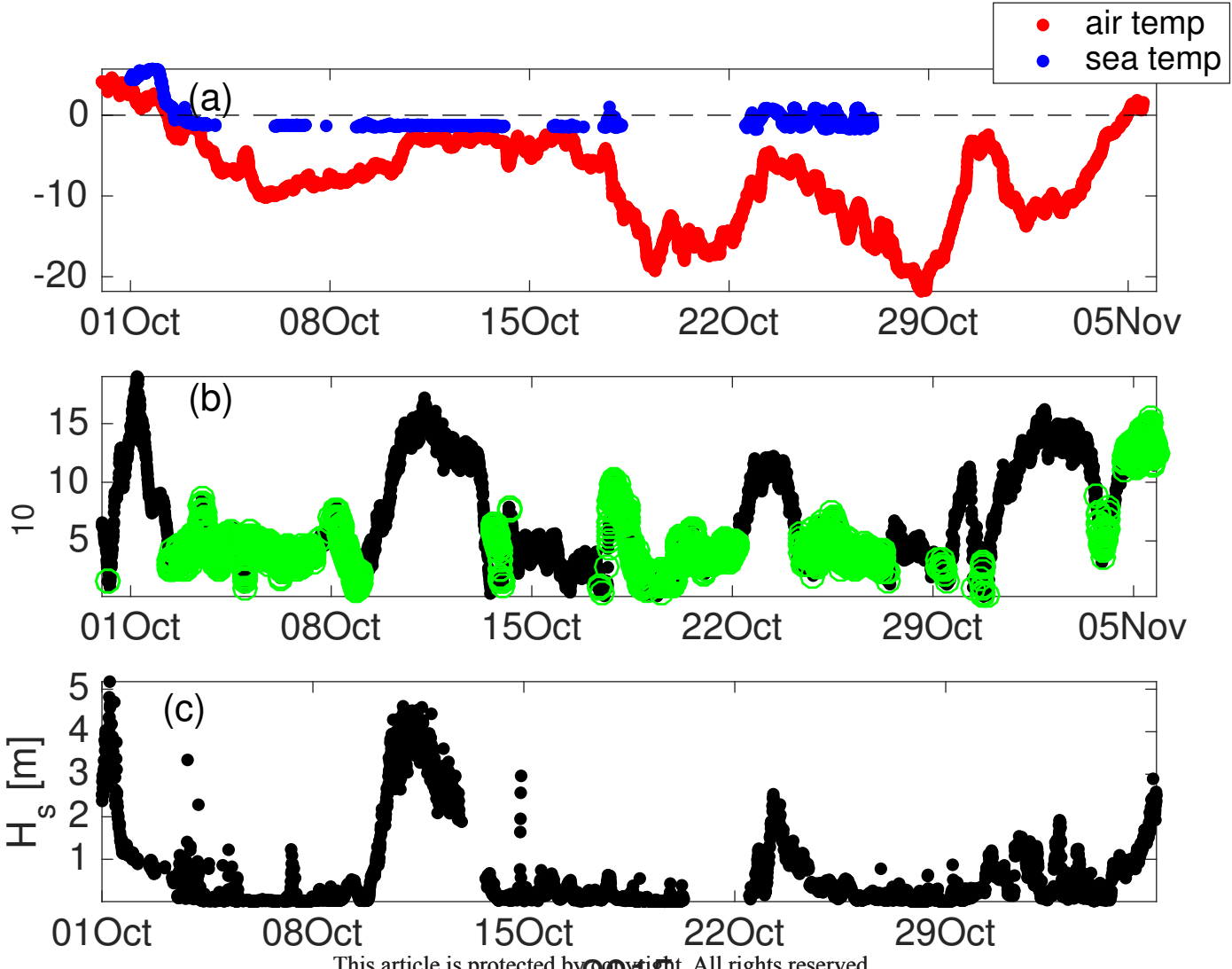

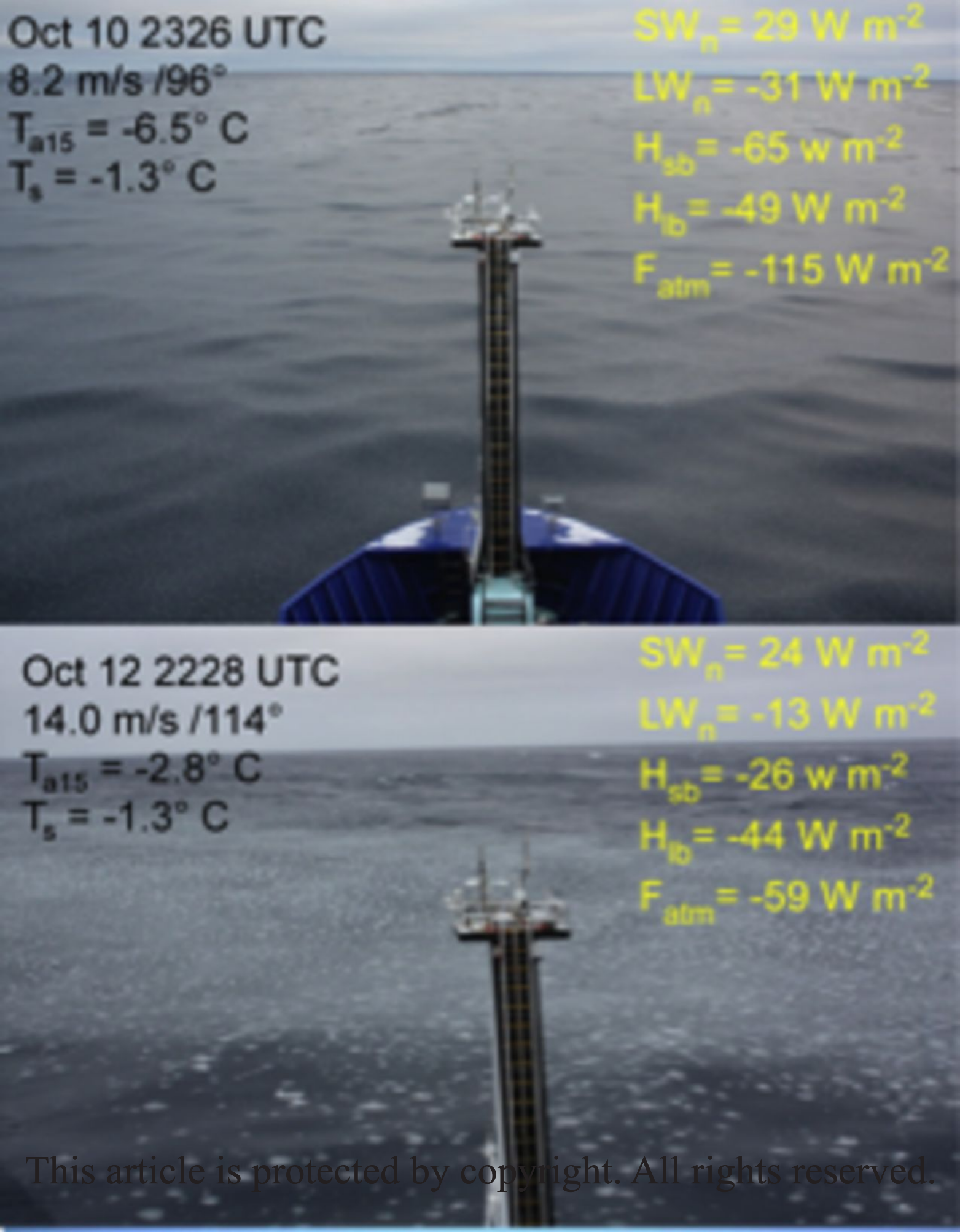

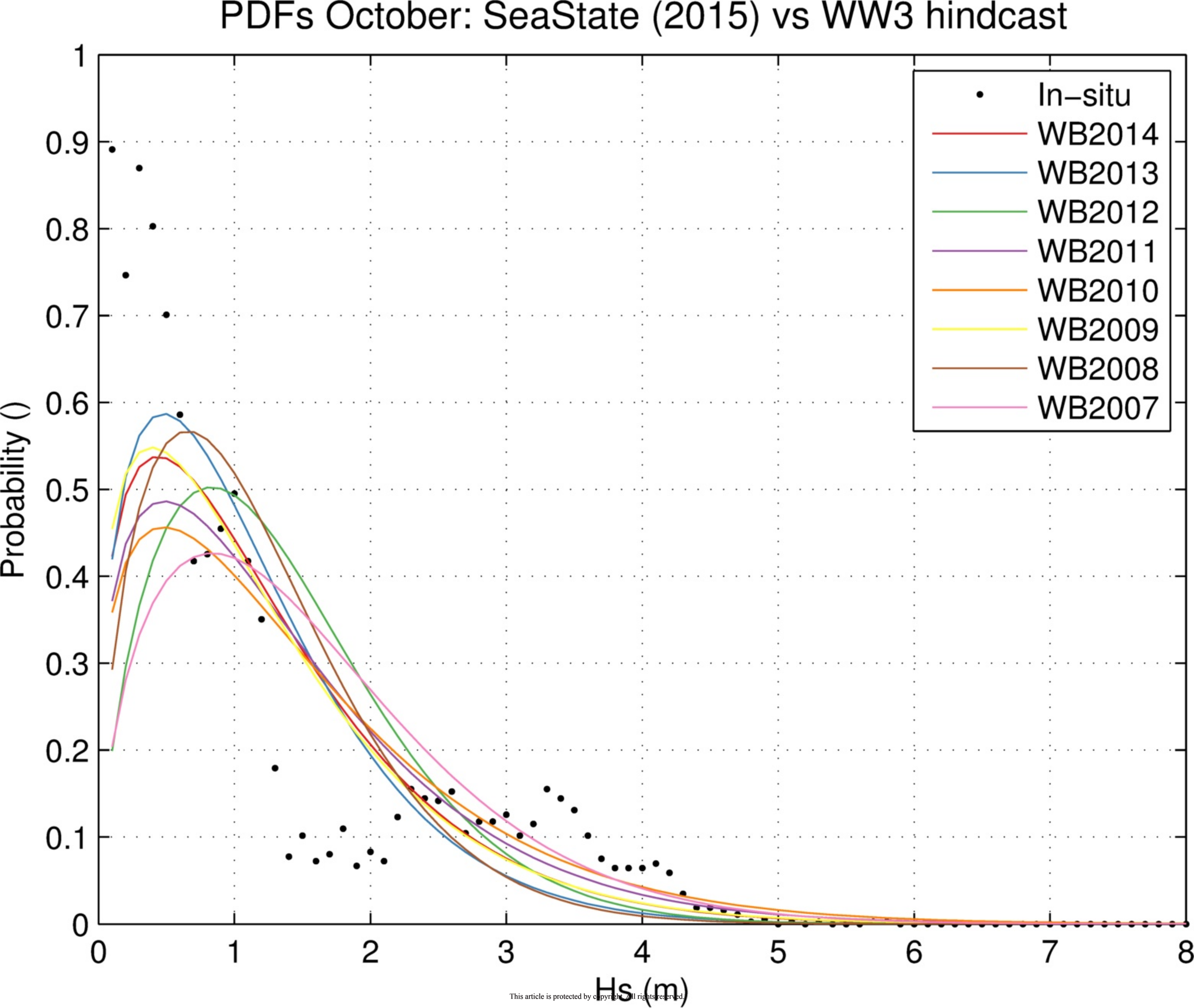

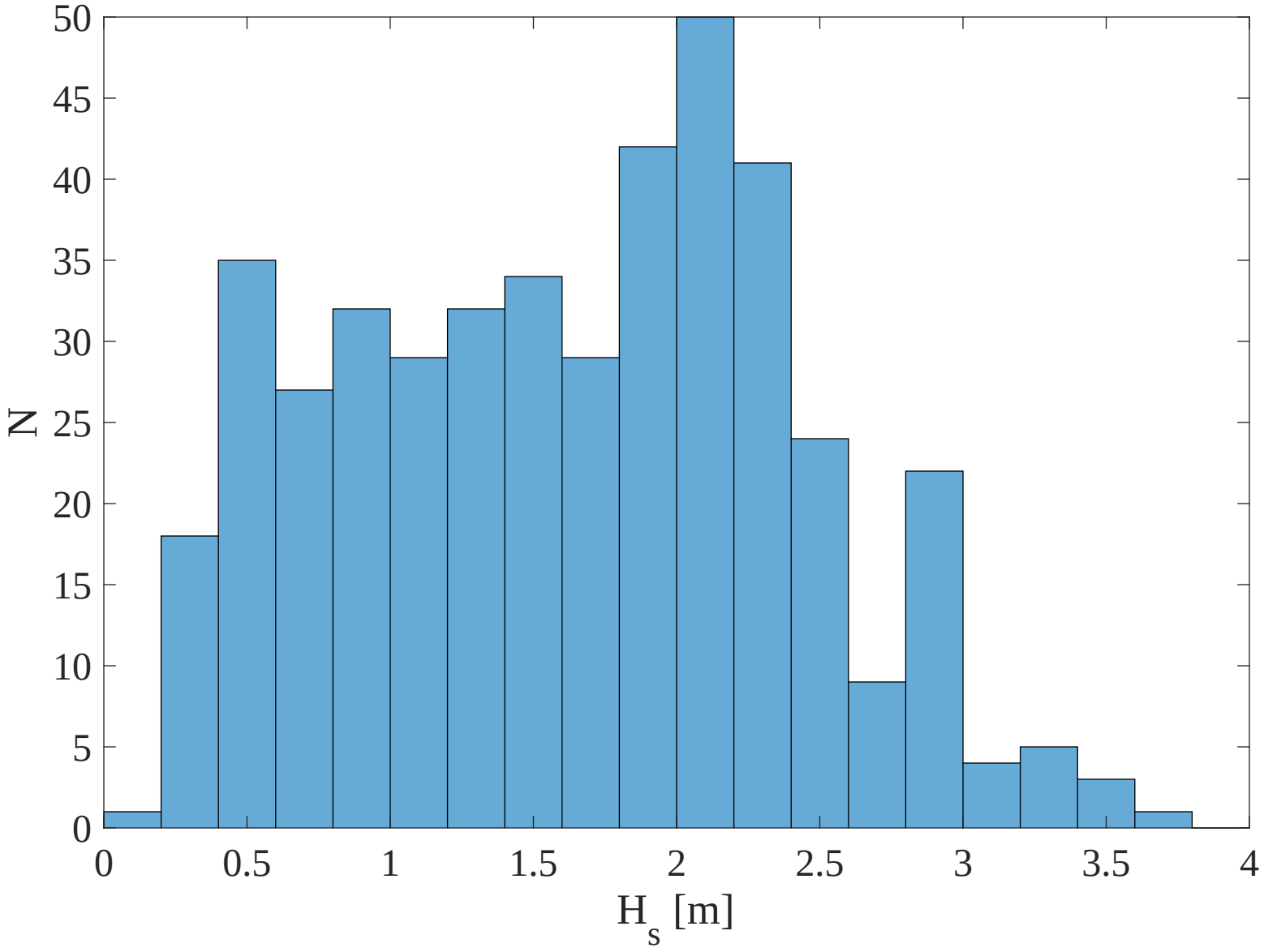

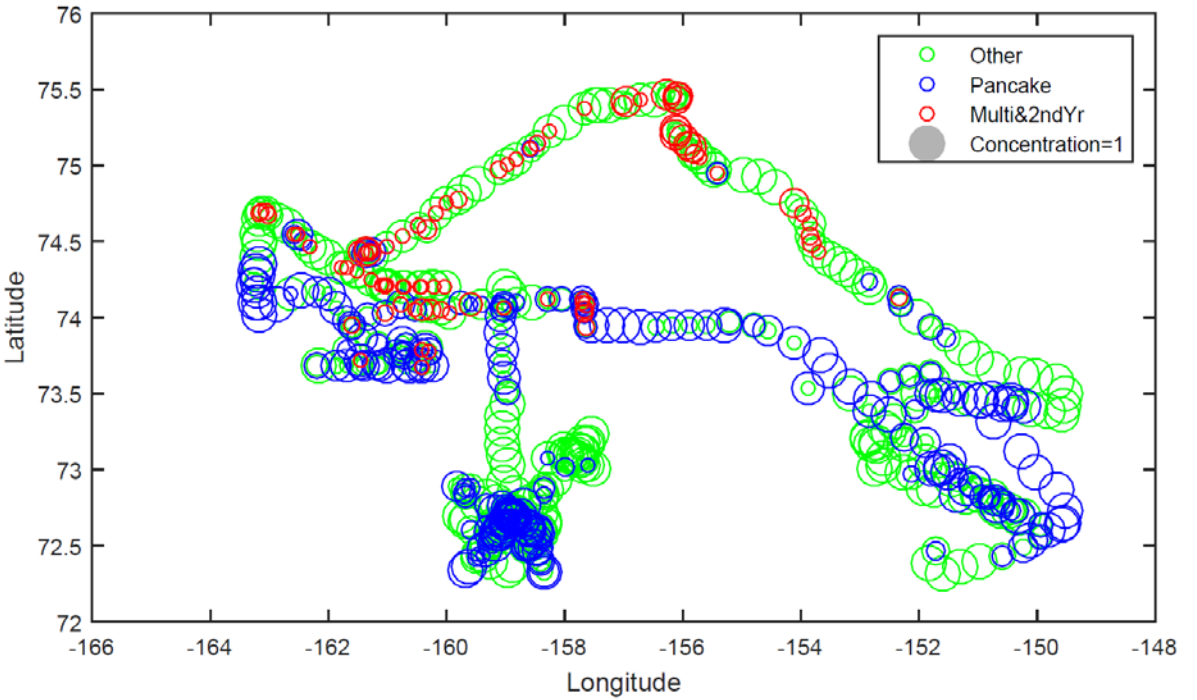
Other
Pancake
Multi&2ndYr
Concentration=1
Latitude
Longitude
76
75.5
75
74.5
74
73.5
73
72.5
72
-166
-164
-162
-160
-158
-156
-154
-152
-150
-148


Multi&2nd Yr


Other


Pancake

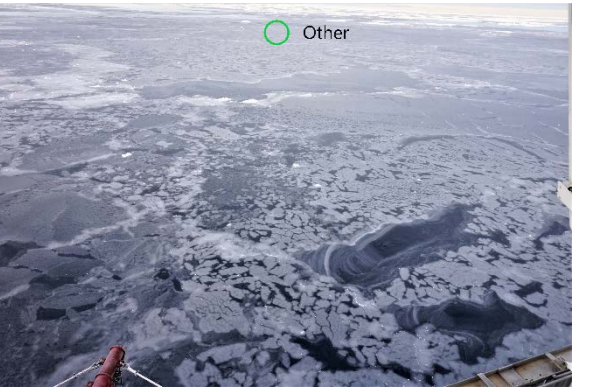
Other

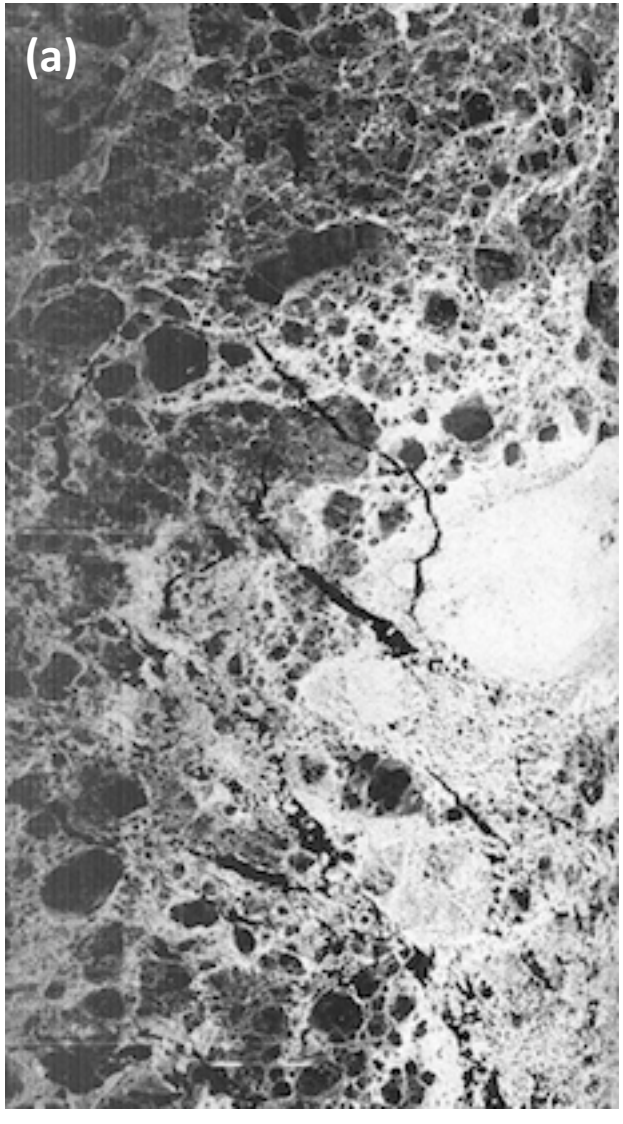
(a)

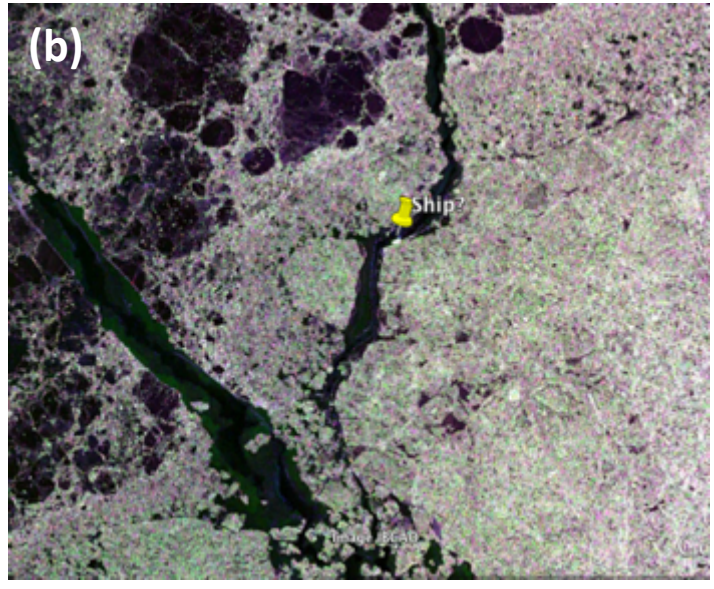
(b)
Ship?

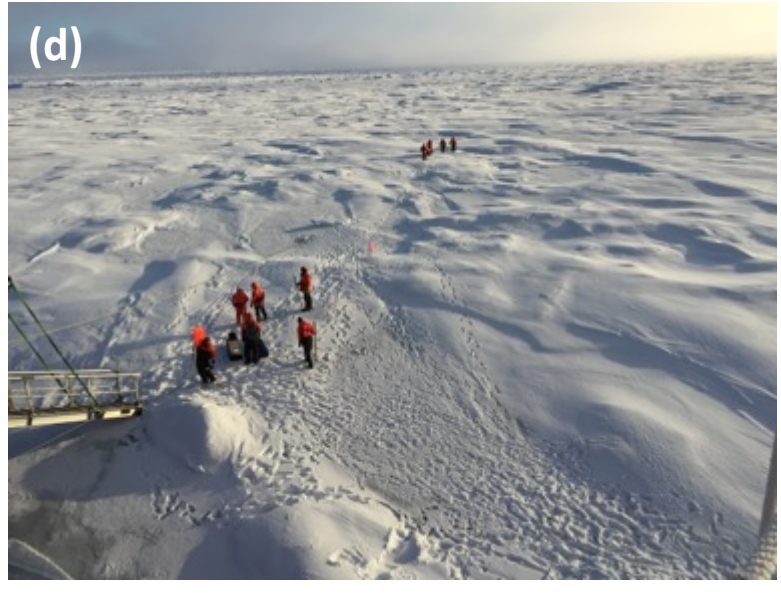
(d)

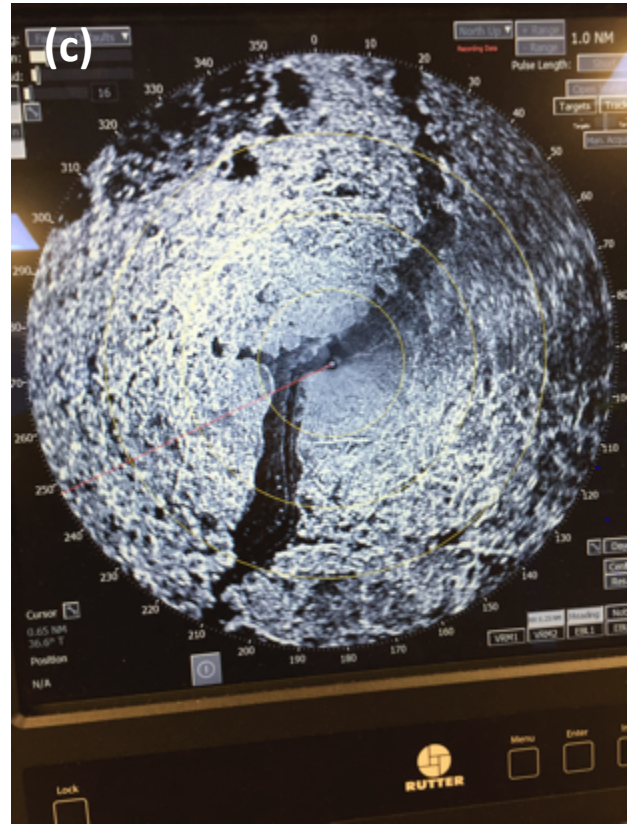
(c)
1.0 NM
Pulse Length
Targets
Cursor
Position
N/A
RUTTER
Menu
Enter
Lock

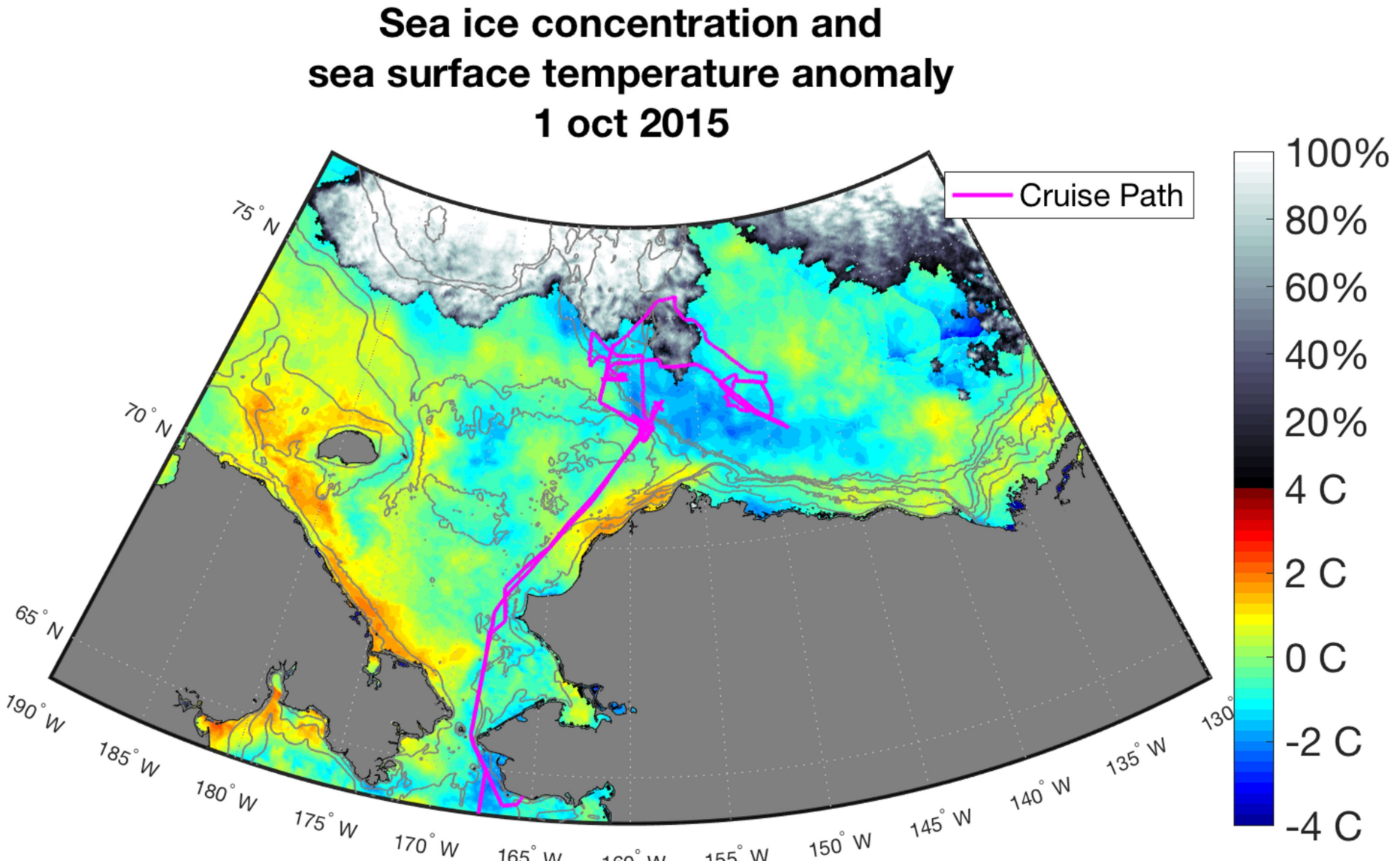

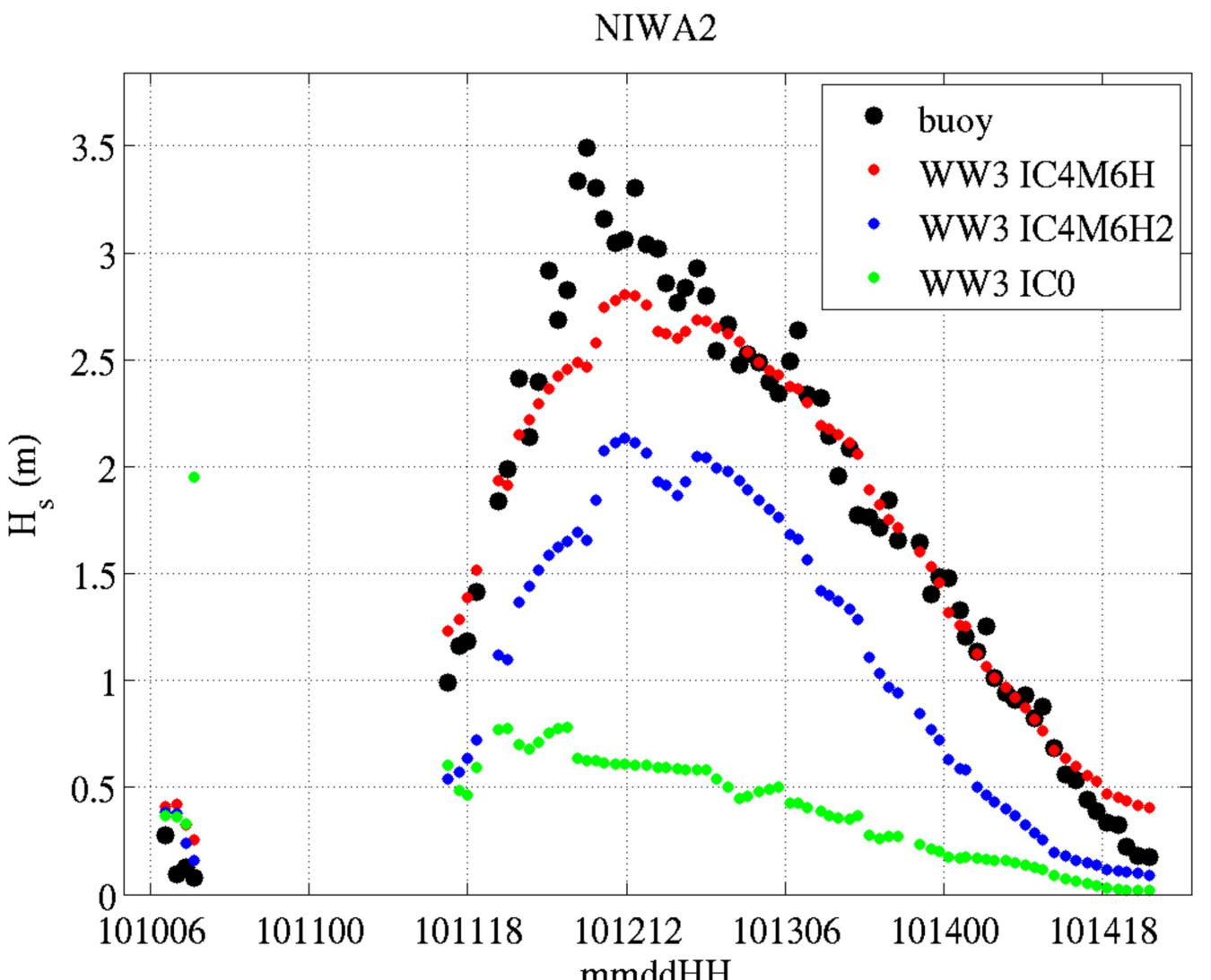

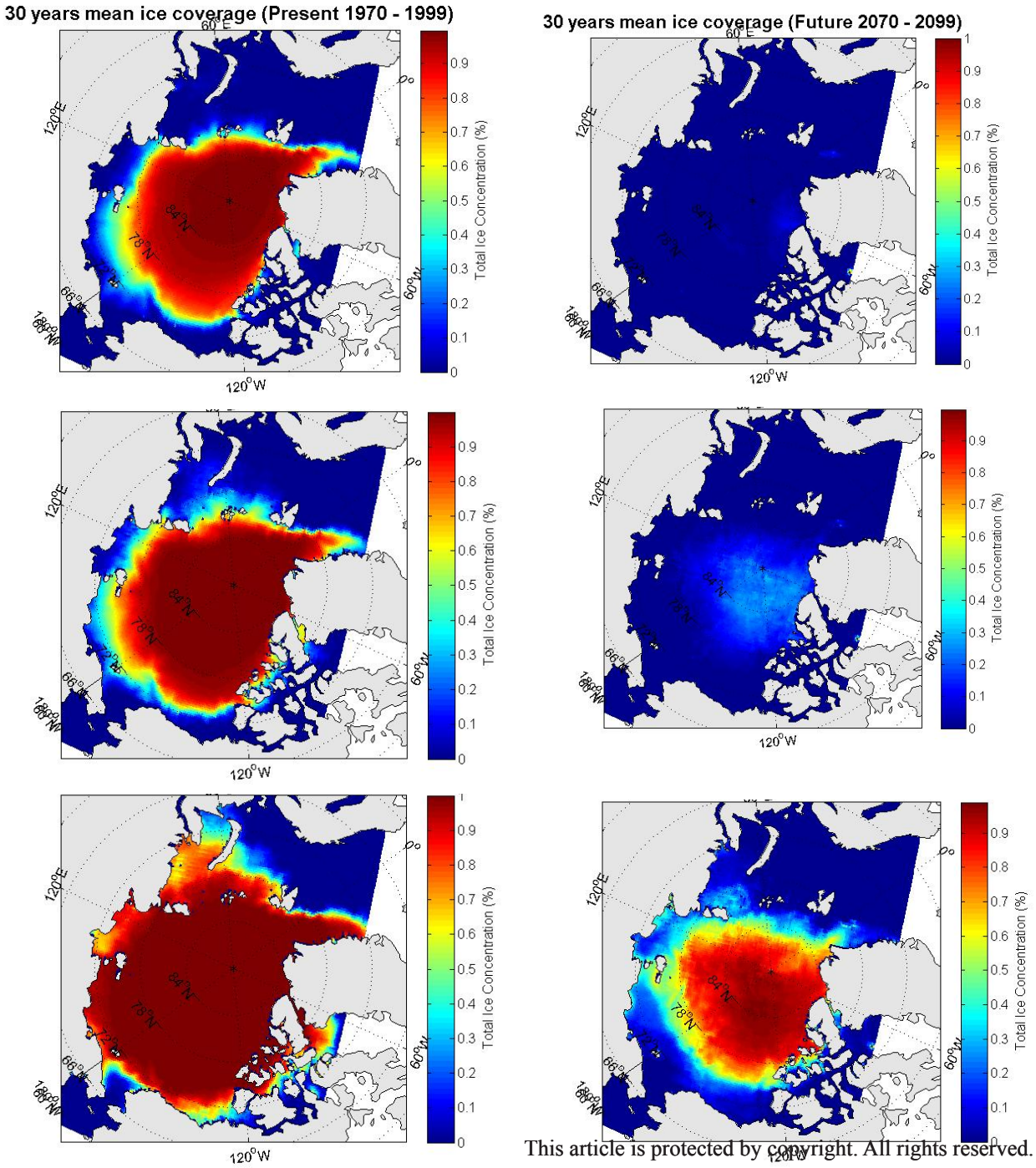

CIOM: A1B scenario

August

October